Power Electronics and Drives
Volume 11(46), 2026 DOI: 10.2478/pead-2026-0001

Power Electronics and Drives

Preventing Magnetic Saturation and Reducing Torque Ripples in Induction Motors Using an Improved Field-Oriented Control System Based on Sliding Mode Technology

Research Paper

Inas Fadhil[1], Alaa Shakir Mahmood[2,*]

[1]*Middle Technical University, Electrical Engineering Technical College, Baghdad, Iraq*
[2]*Middle Technical University, Baghdad, Iraq*

Received: 04 October, 2025; Received in the revised form: 01 December, 2025; Accepted: 08 December, 2025

Abstract: Field-oriented control (FOC) is a widely used strategy that allows independent control of torque and flux in induction motor systems. By applying Park transforms to convert three-phase signals into a dq reference frame, accurate motor speed regulation is achieved while maintaining constant flux for optimal performance and efficiency. Traditional field-oriented control (TFOC) assumes constant rotor resistance; however, variations in this parameter can degrade control accuracy and stability. This research presents an enhanced field-oriented control (EFOC) system that effectively compensates for rotor resistance variations by directly regulating the flux vector in the dq frame, ensuring flux stability and reducing reactive power consumption. Additionally, sliding mode control (SMC) is applied to the outer and inner loops to enhance system robustness, minimise torque ripples and improve dynamic response. Simulation results confirm that the proposed EFOC maintains the flux at its nominal value under resistance changes, achieving a 20% reduction in reactive power, approximately 6% improvement in power factor and reducing torque ripples from 13 N · m^{-1} to 0.3 N · m^{-1}, demonstrating superior performance compared with conventional proportional-integral (PI)-based FOC systems.

Keywords: *induction motor • sliding mode • enhanced field oriented control • flux regulation*

1. Introduction

Induction motors are among the most widely used electric motors because of their great dependability, affordability and extensive application in industrial settings (Faizal et al., 2023; Mahmood and Teke, 2023). They are a cost-effective and sensible option for a variety of industrial applications because of their reputation for dependability and durability, as well as their low maintenance needs (Azzoug et al., 2021; Fereka et al., 2018; Mahmood et al., 2022).

In addition to regulating speed, the key goal of induction motor control systems is to keep the magnetic flux constant, which permits the motor to run at its maximum load capacity while preventing magnetic saturation, thereby increasing operational efficiency and prolonging the motor's service life (Benderradji et al., 2025; Horch et al., 2019; Ramzi et al., 2012). Induction motors can be controlled using various methods. Scalar control, also referred to as V/f control, is the most traditional and still widely used technique. Without taking into account the rotor flux or current, this method modifies the stator voltage's magnitude proportionately to the frequency.

This technique, which controls motor speed or torque by varying the voltage, is straightforward, simple to use and effective under specific circumstances (Mahmood 2024; Sudaryanto et al., 2020). However, V/f control performs poorly dynamically, particularly when there are fluctuating loads or transitory conditions. Because of this, a lot of

* *Email: alaa1984@mtu.edu.iq*

contemporary applications require more sophisticated control systems that can produce nominal torque and retain accurate speed control over the whole operating range.

Conventional V/f systems cannot attain such performance (Online and Citation 2024; Swargiary et al., 2016). More advanced control strategies, such as field-oriented control (FOC), have been created to overcome these constraints (Abed and Zine, 2024; Kumar and Mehar, 2022). For quick dynamic reaction and exact speed and torque control, these techniques rely on precise motor modelling and rotor flux estimation. They are therefore perfect for high-performance applications requiring improved responsiveness and accuracy (El Bourhichi et al., 2021; Peng and Zhao, 2011; Shiravani et al., 2023). However, traditional field-oriented control (TFOC) suffers from a major drawback due to its reliance on motor parameters—particularly the rotor resistance value, which is used to calculate the electrical frequency of the voltage applied to the motor. As a result, any variation in this parameter can lead to a significant deterioration in the motor's steady-state performance (Alaa and Temurtaş, 2024; Mennad et al., 2024). On the other hand, the use of traditional controllers, such as the proportional-integral (PI) controller, may result in poor performance during transient conditions. Therefore, relying on advanced control strategies contributes to improving the motor's performance not only during transients but also in the steady-state regime.

1.1. Related work

Liu and Hao (2006) suggested a sliding mode-based speed controller with an integrated sliding surface to remove the impact of parameter uncertainty on an induction motor's FOC approach. To enhance the performance of the controller, the FOC approach was coupled with the sliding mode control (SMC) strategy.

The FOC technique has been used by Do et al. (2022) to develop an induction motor control architecture on an FPGA platform as a GaN-based control system. Focussing on GaN transistor technology, they were able to increase the switching frequency from 2 kHz to 20 kHz when utilising IGBT transistors of up to 100 kHz. This raises the power converter's power density and drastically lowers switching losses.

Ali et al. (2023) suggested a hybrid speed control algorithm that combines super twisting and backstepping methods to guarantee reliable induction motor speed control under erratic load torque. SMC, super twisting SMC and backstepping control are among the non-linear controllers that are devised. After that, a controller was created that combines the benefits of both backstepping and super twisting SMC approaches to increase robustness and dependability. Through simulations in the MATLAB/Simulink environment, the effectiveness of the design was confirmed by comparing its performance with alternative approaches. Three distinct operating modes—start-stop mode, normal operating mode and disturbance rejection mode—were used to calculate statistical regression coefficients, including integral square of error, integral absolute error and integral absolute error times time.

In the work of Sultan and Al-Badrani (2024), an FOC system is designed to control the seven-phase induction motor speed and rotor flux in the event of a disturbance caused by increased rotor resistance. The control system was developed using two control methods: 1. SMC and 2. Proportional-integral controller (PIC). The results showed that the SMC strategy is able to effectively reduce variations, ensuring that the controlled components remain within the specified reference values, despite changes in parameters.

Shaija and Daniel (2021) addressed the speed control of a three-phase squirrel-cage induction motor using the indirect FOC method. The conventional PIC used in the IFOC system was replaced by an SMC, and the performance of the two methods was compared. Multiple simulation experiments were conducted under various operating conditions using MATLAB/SIMULINK to confirm the effectiveness of the proposed controller. Simulation results showed that the IFOC system using a PI controller offers good steady-state performance, provided the gain coefficients are carefully tuned to suit the operating conditions. Meanwhile, SMC-based control systems exhibit high dynamic performance and are highly robust to external disturbances.

Researchers Marčetić and Vukosavić (2007) proposed a novel method for real-time identification of the rotor time constant in induction motors. The approach is tailored for sensorless, indirect FOC systems that utilise a model reference adaptive system (MRAS) for speed estimation. Instead of injecting test signals, the method takes advantage of the naturally occurring signal fluctuations within the current and speed control loops. The study showed that the phase angle differences between certain spectral components of these small signals can be effectively used to adjust the rotor parameters.

1.2. The scientific problem and research contributions

The conventional FOC relies on only two control loops: one for regulating speed and the other for regulating the flux on the d-axis. These two loops generate the components of the voltage vector, while the frequency is obtained through an algebraic relation that ensures the q-axis flux is equal to zero. However, this relation depends on the rotor resistance value. Therefore, any change in the rotor resistance will cause a degradation in the motor performance.

By adding a third control loop and eliminating the algebraic relation, precise regulation of the q-axis flux can be achieved regardless of variations in rotor resistance. This is what the research aims to demonstrate. This control loop can be implemented using a conventional PIC or using an advanced control strategy, which has not been clearly addressed in the related research works such as Alaa and Temurtaş (2024) and Shaija and Daniel (2021).

On the other hand, studies by Do et al. (2022), Liu and Hao (2006) and Shaija and Daniel (2021) have primarily concentrated on improving speed and torque performance, often neglecting the accurate regulation of the magnetic flux component along the q-axis—an aspect that is crucial for minimising reactive power consumption and enhancing system efficiency.

Although Liu and Hao (2006) and Ali et al. (2023) introduced a non-linear control strategy including SMC, super twisting algorithms and backstepping have been explored in the dynamic effects of rotor parameter variations, particularly rotor resistance overall system stability and accuracy remain under-investigated.

Although Marčetić and Vukosavić (2007) introduced a novel method for real-time identification of the rotor time constant using MRAS estimators, such techniques were not integrated into a complete adaptive control framework capable of responding effectively to parameter changes during operation.

Comparative studies, such as those of Ali et al. (2023) and Shaija and Daniel (2021) evaluate performance under limited operating conditions and focus on a narrow range of indicators, often excluding key performance metrics such as torque ripple, load tolerance and reactive power variation. Furthermore, reliance on conventional PI controllers in works like Sultan and Al-Badrani (2024) and Marčetić and Vukosavić (2007) demonstrates limited robustness under non-linear disturbances and lacks adaptability in dynamic scenarios.

Table 1 shows a comparison between previous studies and identifies the shortcomings in each of them.

In light of these identified gaps, the present study proposes an improved FOC scheme that incorporates a dedicated control loop to regulate the q-axis flux component, ensuring it remains at zero in the steady state. This enhancement is evaluated in conjunction with both PI and SMC strategies under various operating conditions, including rotor resistance variations and external load disturbances, with a focus on comprehensive performance indicators such as settling time, torque ripple, reactive power and load handling capacity.

Table 1. Comparative summary of related studies.

Study	Control strategy	Main focus	Limitation/gap identified
Alaa and Temurtaş (2024)	SMC and FLC	Improve speed and torque performance	A sufficient analysis regarding the effect of changes in rotor resistance was not provided. It was not demonstrated that good flux regulation can be achieved even with a PIC. The control system is relatively complex. The effect of saturation on reactive power draw was not discussed.
Shaija and Daniel (2021)	SMC	Improve the robustness of torque and speed control	Accurate q-axis flux regulation is not addressed. The effect of saturation on reactive power draw was not discussed.
Do et al. (2022)	PI controllers	Improve the dynamic response of speed and torque	Accurate q-axis flux regulation is not addressed. The system's performance was not discussed in light of changes in the rotor resistance value.
Ali et al. (2023)	Non-linear controllers (SMC, super-twisting, backstepping)	Increase robustness under disturbances	The effect of rotor resistance variation has not been deeply analysed. The control system is relatively complex.
Sultan and Al-Badrani (2024)	PI and SMC controllers	Compare controller performance under limited conditions	Limited robustness and adaptability in non-linear operating conditions. The system's performance was not discussed in light of changes in the rotor resistance value. The effect of saturation on reactive power draw was not discussed.

PI, proportional-integral; PIC, proportional-integral controller; SMC, sliding mode control.

This research aims to address these issues in the following ways:

- Study the effect of changing the rotor resistance value on the performance of the traditional FOC system, and analyse the control signals and compare them with the case of using the enhanced FOC system;
- Develop an enhanced flux vector control system where the magnetic flux is precisely regulated, ensuring that the rotor flux component on the q-axis remains regulated at zero in the steady state. This is achieved by adding a control loop to regulate it, which enhances operational efficiency and reduces reactive power consumption;
- Improve control system performance and reduce torque ripples.

Accordingly, four control systems were studied and presented, as follows:

- The first control system is a traditional flux-oriented control system based on PICs (TFOC-PI).
- The second control system is an enhanced flux-oriented control system based on PICs (EFOC-PI).
- The third control system is a traditional flux-oriented control system based on a sliding mode controller (TFOC-SM).
- The fourth control system is an enhanced flux-oriented control system based on a sliding mode controller (EFOC-SM).

The research will evaluate the performance of these four systems under operating conditions, including changes in rotor resistance, load torque, settling time, torque ripple, load tolerance and reactive power consumption.

2. The Dynamic Model of the Induction Motor

The dq reference frame is used to transform the 3-phase motor equations from the three-phase system into a two-phase equivalent system, simplifying analysis and control. This transformation allows the torque and magnetic flux components to be separated, facilitating the design of precise control systems such as vector control. The representation in a dq frame of a three-phase induction motor is (Mahmood 2024; Mennad et al., 2024) as follows:

$$\frac{\mathrm{d}i_{sd}}{\mathrm{dt}} = -a_5 i_{sd} + \omega_s i_{sq} + a_3 \Phi_{rd} + a_4 \omega \Phi_{rq} + b v_{sd} \tag{1}$$

$$\frac{\mathrm{D}i_{sq}}{\mathrm{dt}} = -\omega_s i_{sd} - a_5 i_{sq} - a_4 \omega \Phi_{rd} + a_3 \Phi_{rq} + b v_{sq} \tag{2}$$

$$\frac{\mathrm{d}\Phi_{\mathrm{rd}}}{\mathrm{dt}} = a_2 R_r i_{sd} - a_1 \Phi_{rd} + (\omega_s - \omega)\Phi_{rq} \tag{3}$$

$$\frac{\mathrm{d}\Phi_{\mathrm{rq}}}{\mathrm{dt}} = a_2 R_r i_{sq} - (\omega_s - \omega)\Phi_{rd} - a_1 \Phi_{rq} \tag{4}$$

$$\frac{d\omega}{dt} = \frac{p}{J}\left(G\Phi_{rd} i_{sq} - G\Phi_{rq} i_{sd} - T_L\right) - \frac{f}{J}\omega \tag{5}$$

The D–Q reference frame for a dynamic motor model explains how the motor's mechanical speed, rotor fluxes and stator currents are physically related.

Where: $a_1 = \frac{R_r}{L_r}, a_2 = \frac{L_m}{L_r}, a_3 = \frac{L_m R_r}{\sigma L_s L_r^2}, a_4 = \frac{L_m}{\sigma L_s L_r}, a_5 = \frac{L_r^2 R_s + L_m^2 R_r}{\sigma L_s L_r^2},$

$$b = \frac{1}{\sigma L_s}, G = \frac{P L_m}{L_r}, \sigma = 1 - \frac{L_m^2}{L_s L_r},\ \omega = p\Omega$$

To convert electrical signals from a three-axis frame into a dq frame rotating at synchronous speed, the following Park transform matrix is used:

$$\begin{bmatrix} X_d \\ X_q \\ X_0 \end{bmatrix} = \sqrt{\frac{2}{3}} \begin{bmatrix} \cos(\theta_s) & \cos\left(\theta_s - \frac{2\pi}{3}\right) & \cos\left(\theta_s + \frac{2\pi}{3}\right) \\ -\sin(\theta_s) & -\sin\left(\theta_s - \frac{2\pi}{3}\right) & -\sin\left(\theta_s + \frac{2\pi}{3}\right) \\ \frac{1}{\sqrt{2}} & \frac{1}{\sqrt{2}} & \frac{1}{\sqrt{2}} \end{bmatrix} \begin{bmatrix} X_a \\ X_b \\ X_c \end{bmatrix} \tag{6}$$

Where: $\theta_s = \int \omega_s dt$.

The induction motor's dynamic model was created in MATLAB-Simulink using the parameters listed in Table 2.

3. FOC-Based Control System of IM Using a PI Controller

The FOC method is used in an AC motor control system to dissociate flux control from torque control. This is done by aligning the rotor flux vector with the d-axis, and the rotor flux component on the q-axis is kept constant at zero. That makes the link between the flux and torque linear. This method enables the motor's torque and rotor flux components to be independently controlled and manipulated (Mennad et al., 2024; Swargiary et al., 2016) as follows:

$$\Phi_r = \Phi_{rd}, \ \Phi_{rq} = \frac{d\Phi_{rq}}{dt} = 0 \tag{7}$$

Park conversion and field orientation situation (Eq. (6)) converts measured three-phase values into the dq frame that rotates. In Eq. (7), it is shown that the rotor flux requires to be precisely aligned with the d-axis, which means that the flux on the q-axis must be zero.

Using the two previous assumptions and neglecting internal disturbances, Eqs (1)–(5) can be written as follows:

Table 2. Listing all symbols, abbreviations and constants.

Symbol	Description	Unit
ω_S	Synchronous speed (electrical frequency)	rad · s^{-1}
ω	Electric speed	rad · s^{-1}
v_{sq}, v_{sd}	Stator voltage vector on q and d-axis	V
i_{sq}, i_{sd}	Stator current vector on q and d-axis	A
Φ_{rq}, Φ_{rd}	Rotor flux vector on q and d-axis	Wb
P	Number of pole pairs	-
L_s	Stator inductance	H
L_r	Rotor inductance	H
L_m	Magnetizing inductance	H
R_S	Stator resistance	Ω
R_r	Rotor resistance	Ω
F	Friction coefficient	N · m^{-1} · s^{-1}
J	Rotor inertia	kg · m^{-2}
T_L	Load torque	N · m^{-1}
T_e	Electromagnetic torque	N · m^{-1}
V_{dc}	DC link voltage	V
Ω	Mechanical speed	rad · s^{-1}

$$\frac{di_{sd}}{dt} = -a_5 i_{sd} + bv_{sd} \quad (8)$$

$$\frac{di_{sq}}{dt} = -a_5 i_{sq} + bV_{sq} \quad (9)$$

$$\frac{d\Phi_{rd}}{dt} = a_2 R_r i_{sd} - a_1 \Phi_{rd} \quad (10)$$

$$\frac{d\omega}{dt} = \frac{pG\Phi_{rd}}{J} i_{sq} - \frac{f}{J}\omega \quad (11)$$

FOC equations are made simpler. These show the dynamics of the motor under the assumption of perfect decoupling and constant motor settings.

As shown in Figure 1, it may depict the induction motor concept in a FOC-based dq frame.

To convert electrical signals from an abc-frame to a dq-frame, the oriented angle must be obtained, which is the integral of the synchronous speed. To achieve synchronous speed, relationship Eq. (4) can be configured as follows:

$$\omega_s = \omega + \omega_{slip}, \ \omega_{slip} = \frac{a_2 R_r}{\Phi_{rd}} i_{sq} \quad (12)$$

3.1. Conceptual illustration of the enhanced field-oriented control framework

Figure 2 illustrates the proposed field-enhanced control enhanced field-oriented control (EFOC) system for the conceptual framework of an induction motor. The speed control loop, the d-axis flux control loop and the q-axis flux control loop vector are the main control loops that comprise the control system. To maintain precise separation between the d and q axes, optimise dynamic response and ensure robustness against rotor resistance fluctuations, measured feedback signals for both speed and the two components of the flux vector are used. The controllers process the flux and speed reference signals (ω, Φ_d, Φ_q) to generate both the components of the voltage vector (V_d, V_q) and the electrical frequency. Integrating the frequency signal yields the orientation angle, which is used within Park transform equations to convert the voltage vector components into three-phase voltage signals. These are then processed in a sinusoidal pulse-width modulation (SPWM) stage to obtain the pulses applied to the inverter that powers the motor.

In the drive system, a two-level inverter was used, where the output voltages are determined based on the state of the electronic switches and the DC-link voltage (V_{dc}) value according to the following equations:

$$\begin{bmatrix} V_a \\ V_b \\ V_c \end{bmatrix} = \frac{V_{dc}}{3} \begin{bmatrix} 2 & -1 & -1 \\ -1 & 2 & -1 \\ -1 & -1 & 2 \end{bmatrix} \begin{bmatrix} C_a \\ C_b \\ C_c \end{bmatrix}$$

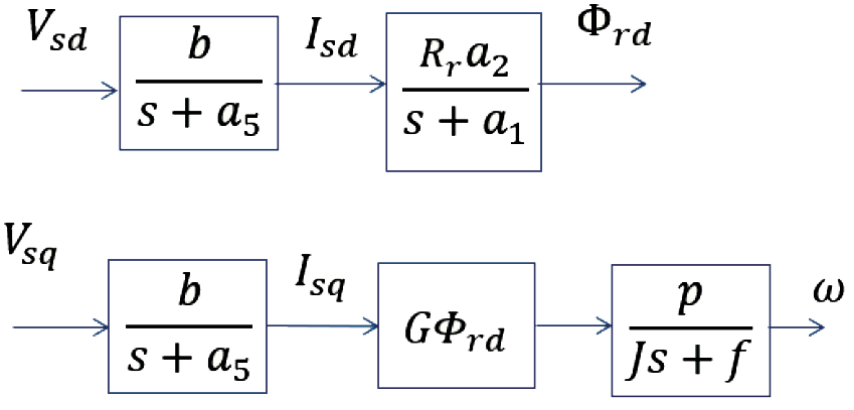

Figure 1. The block diagram of an induction motor in the dq frame.

In fact, for the proposed drive system, a three-level or five-level inverter can be used, taking into account the necessary adjustment to be applied during the SPWM.

3.2. TFOC control using PI controller

The most common method for powering electrical machines and control systems is the PI controller, which is straightforward to use. They do, however, have several disadvantages that may produce unforeseen outcomes. Figure 3 shows an illustration of TFOC employing PI controllers.

3.3. EFOC control using PI controller

Any change in the rotor resistance value will lead to failure in the traditional control system. This change must be compensated for in the relationship 12 to obtain the optimal value for the synchronous speed, which actually represents the electrical frequency of the voltage applied to the motor. Therefore, in this research, we seek to eliminate this problem by adding a third control loop, through which errors resulting from a change in the rotor resistance value are corrected.

Reviewing Eq. (4), considering the synchronous speed as the control signal and considering the magnetic flux along the q-axis as a state variable, and neglecting disturbance ($a_2 R_r i_{sq}$), this relationship becomes:

$$\frac{d\Phi_{rq}}{dt} = -(\omega_s - \omega)\Phi_{rd} - a_1 \Phi_{rq} \tag{13}$$

Flux error dynamics and slip speed calculation (Eq. (12)) determine the necessary synchronous speed using the nominal rotor resistance. Eq. (13) illustrates how a deviation in the nominal motor resistance affects the q-axis flux error.

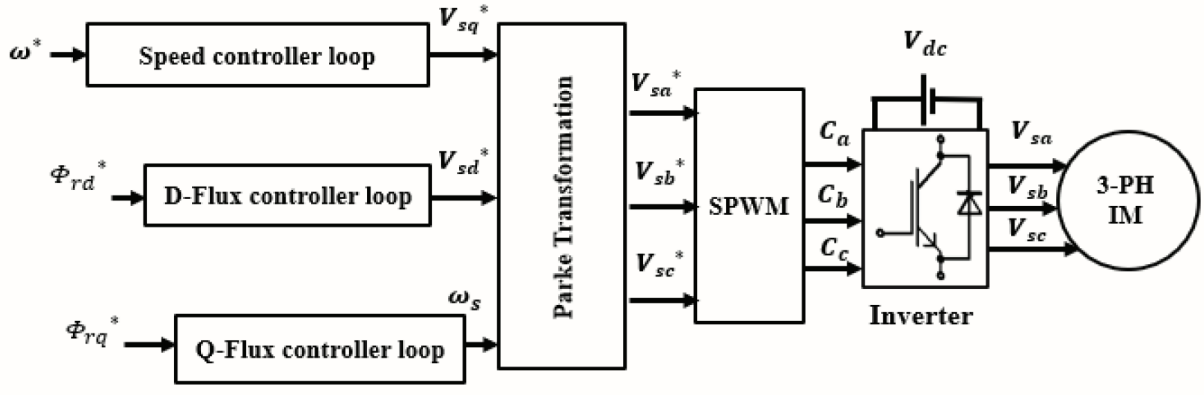

Figure 2. Conceptual block diagram of the proposed EFOC system. EFOC, enhanced field-oriented control.

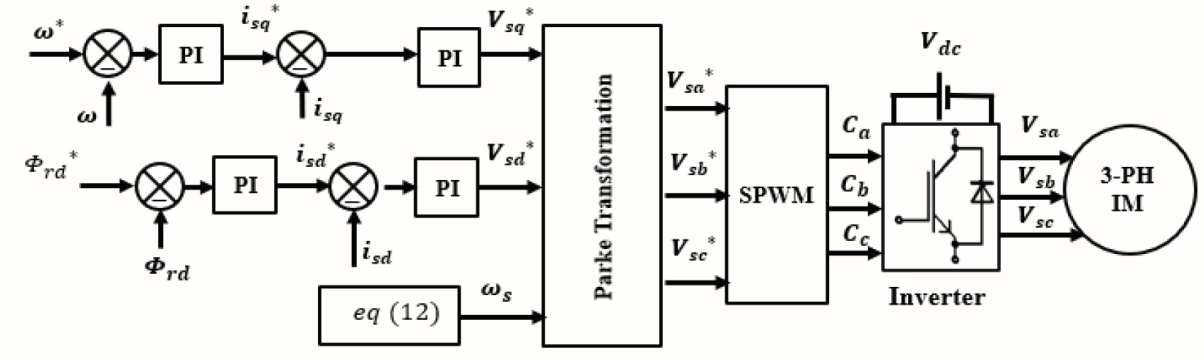

Figure 3. The illustration of TFOC using PI controllers. PI, proportional-integral; SPWM, sinusoidal pulse-width modulation; TFOC, traditional field-oriented control.

It can formulate the transfer function shown in Figure 4, which represents the correlation map between the frequency and magnetic flux along the q-axis as follows:

Figure 5 shows the illustration of the EFOC using PI controllers, which includes a third control loop.

3.4. TFOC control using SM controller

Upon reviewing the motor's dynamic Eqs (1)–(5), we observe the presence of non-linear terms, such as the term $\omega_s i_{sd}$ in the first equation, which represents the product of the state variable i_{sd} and the control signal ω_s, and the term $a_4 \omega \Phi_{rq}$ representing the product of two state variables. Similarly, in the second equation, we observe the term $a_4 \omega \Phi_{rd}$ that is also a product of two state variables and another representing the product of a state variable and a control signal $\omega_s i_{sd}$. Furthermore, the fifth equation contains a product of two state variables $\Phi_{rd} i_{sq}$ and another product of two state variables $\Phi_{rq} i_{sd}$.

The robustness, insensitivity to changes in machine parameters, simplicity of use, robust dynamic performance, and stability under erratic and quickly shifting circumstances are the hallmarks of SMC. SMC, in contrast to traditional linear controllers, can deal with non-linearities and model errors with little loss of control quality. Its use has grown in many fields, including power electronics, robotics and electric motor control systems (Shaija and Daniel, 2021; Sultan and Al-Badrani, 2024 and Rahmatullah et al., 2023).

3.4.1. SMC design steps

It is known that the sliding-type control law has two parts: the first part represents the equivalent control (keeps the system on the surface). The second part is the attraction control that is used to push the system towards the surface.

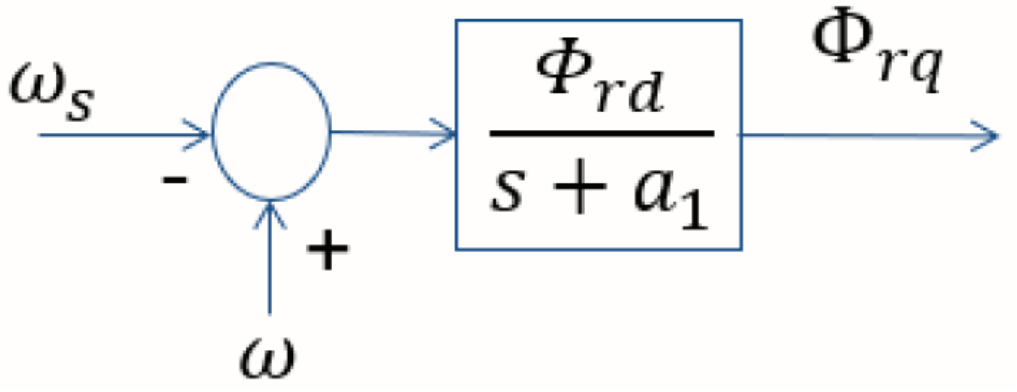

Figure 4. The map between frequency and magnetic flux.

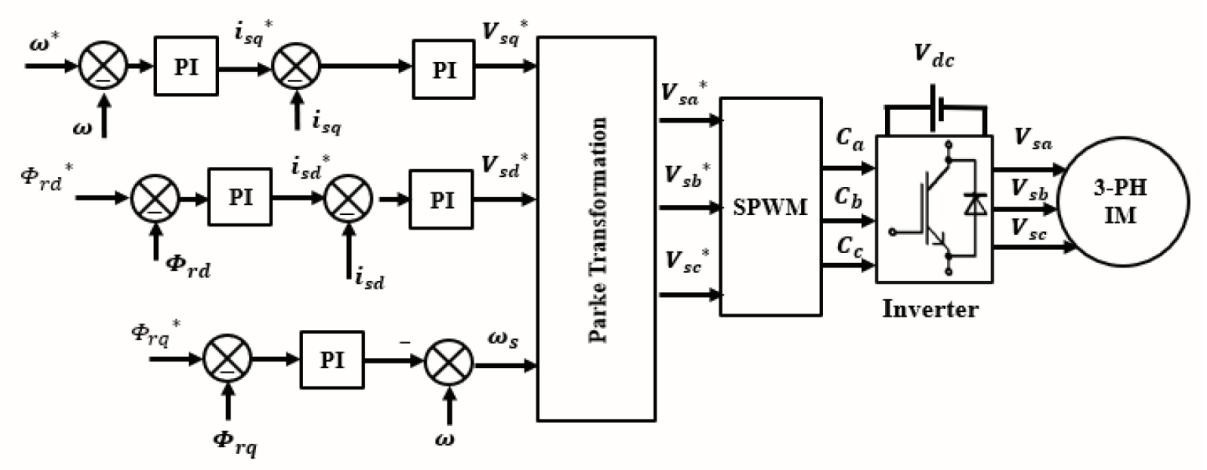

Figure 5. The illustration of EFOC using PI controllers. EFOC, enhanced field-oriented control; PI, proportional-integral; SPWM, sinusoidal pulse-width modulation.

A stability system is described as the following differential equation:

$$\dot{x} = Ax + Bu \tag{a}$$

The sliding surface was adopted as representing the error signal as follows:

$$S = x_{\text{ref}} - x \tag{b}$$

The reference signal can be considered to have a fixed value and equal to zero:

$$S = -x \tag{c}$$

$$\therefore \dot{S} = -\dot{x} \tag{d}$$

The law control was chosen to be as follows:

$$\dot{S} = -K_1 Sgn(S) - K_2(s) \tag{e}$$

By equating the two relationships (b and c), we find

$$-Ax - Bu = -K_1 Sgn(S) - K_2(s) \tag{f}$$

$$\therefore u = -\frac{A}{B}x + \frac{K_1}{B}Sgn(S) + \frac{K_2}{B}(s) \tag{g}$$

It is noted that the control law consists of two parts, as we mentioned previously, the equivalent control $\left(-\frac{A}{B}x\right)$ and the attraction control $\left(\frac{K_1}{B}Sgn(S) + \frac{K_2}{B}(s)\right)$.

3.4.2. System stability analysis

For a given Lyapunov function according to the equation:

$$V = 0.5S^2 \tag{h}$$

In order for the system to be stable, the following must be achieved:

$$\dot{V} = \dot{S}S < 0 \tag{i}$$

$$\therefore -K_1 Sgn(S)S - K_2(s)S < 0 \tag{j}$$

To satisfy the condition in Eq. (j) the constants (K_1, K_2) must be a positive value, and this ensures the stability of the system.

3.4.3. Regulation of I_{sd} current

The I_{sd} current-regulating loop's switching surface can be expressed as

$$\boldsymbol{S}_{\text{id}} = I_{\text{sd-ref}} - I_{\text{sd}} \tag{14}$$

By deriving the previous relationship, based on Eq. (8), we find:

$$\dot{S}_{\text{id}} = \frac{\boldsymbol{dI}_{\text{sd-ref}}}{\boldsymbol{dt}} + \boldsymbol{a}_5 i_{\text{sd}} - \text{bV}_{\text{sd}} \tag{15}$$

An adequate law of attraction must compensate for $\dot{S}_{\text{id}}$ to force the current to travel towards the sliding surface:

$$\dot{S}_{\mathrm{id}} = -\boldsymbol{K}_1 \mathrm{sig}\mathrm{S}_{\mathrm{id}} - \boldsymbol{Q}_1 S_{\mathrm{id}} \tag{16}$$

By equating relations Eqs (15) and (16), we get:

$$\boldsymbol{V}_{\mathrm{sd}} = \frac{1}{\boldsymbol{b}}\left(\frac{\boldsymbol{dI}_{\mathrm{sd-ref}}}{\boldsymbol{dt}} + \boldsymbol{a}_5 i_{\mathrm{sd}} + \boldsymbol{K}_1 \mathrm{sig} S_{\mathrm{id}} + \boldsymbol{Q}_1 S_{\mathrm{id}} \right) \tag{17}$$

3.4.4. Regulation of I_{sq} current

The I_{sq} current-regulating loop's switching surface can be expressed as

$$\boldsymbol{S}_{\mathrm{iq}} = I_{sq-\mathrm{ref}} - I_{\mathrm{sq}} \tag{18}$$

By deriving the previous relationship and based on Eq. (9), we find:

$$\dot{S}_{\mathrm{iq}} = \frac{\boldsymbol{dI}_{\mathrm{sq-ref}}}{\boldsymbol{dt}} + \boldsymbol{a}_5 i_{\mathrm{sq}} - \mathrm{bV}_{\mathrm{sq}} \tag{19}$$

An adequate law of attraction must compensate for $\dot{S}_{\mathrm{iq}}$ to force the stream to travel towards the sliding surface:

$$\dot{S}_{\mathrm{iq}} = -\boldsymbol{K}_2 \mathrm{sig}\mathrm{S}_{iq} - \boldsymbol{Q}_2 S_{iq} \tag{20}$$

By equating relations Eqs (19) and (20), we get:

$$\boldsymbol{V}_{\mathrm{sq}} = \frac{1}{\boldsymbol{b}}\left(\frac{\boldsymbol{dI}_{\mathrm{sq-ref}}}{\boldsymbol{dt}} + \boldsymbol{a}_5 i_{sq} + \boldsymbol{K}_2 \mathrm{sig} S_{\mathrm{iq}} + \boldsymbol{Q}_2 S_{\mathrm{iq}} \right) \tag{21}$$

For Inner Current Loops (D-axis current and Q-axis current), SMC defines the sliding surfaces and determines the voltage control laws required to provide quick and precise current tracking.

3.4.5. Regulation of Φ_{rd}

The Φ_{rd} regulating loop's switching surface can be expressed as

$$\boldsymbol{S}_{\mathrm{d}} = \boldsymbol{\Phi}_{\boldsymbol{rd}-ref} - \boldsymbol{\Phi}_{\boldsymbol{rd}-ref} \tag{22}$$

By deriving the previous relationship, and based on Eq. (10), we find:

$$\dot{S}_{\mathrm{d}} = \Phi_{\boldsymbol{rd}-ref} - \boldsymbol{a}_2 R_r i_{sd} + \boldsymbol{a}_1 \Phi_{rd} - \left(\boldsymbol{\omega}_s - \boldsymbol{\omega}\right)\boldsymbol{\Phi}_{rq} \tag{23}$$

An adequate law of attraction must compensate for $\dot{S}_{\mathrm{iq}}$ to force the stream to travel towards the sliding surface:

$$\dot{S}_{\mathrm{d}} = -\boldsymbol{K}_3 \mathrm{sig}(\mathbf{S}_{\mathrm{d}}) - \boldsymbol{Q}_3(\mathbf{S}_{\mathrm{d}}) \tag{24}$$

By equating relations Eqs (18) and (14), we get:

$$\boldsymbol{i}_{\boldsymbol{sd}-ref} = \left(\dot{\Phi}_{\boldsymbol{rd}-ref} + \boldsymbol{a}_1 \Phi_{rd} - \left(\omega_s - \omega\right)\Phi_{rq} + \boldsymbol{K}_3 \mathrm{sig}(\mathbf{S}_{\mathrm{d}}) + \boldsymbol{Q}_3(\mathbf{S}_{\mathrm{d}})\right) / \left(\boldsymbol{a}_2 R_r\right) \tag{25}$$

3.4.6. Regulation of speed

The speed regulating loop's switching surface can be expressed as

$$\boldsymbol{S}_{\boldsymbol{\omega}} = \omega_{\mathrm{ref}} - \boldsymbol{\omega} \tag{26}$$

By deriving the previous relationship, and based on Eq. (11), we get:

$$\dot{S}_{\omega} = \dot{\omega}_{\text{ref}} - \frac{pG\Phi_{rd}}{J} i_{sq} + \frac{f}{J}\omega \tag{27}$$

An adequate law of attraction must compensate for $\dot{S}_{\omega}$ in order to force the stream to travel towards the sliding surface:

$$\dot{S}_{\omega} = -K_4 \text{sig}(S_{\omega}) - Q_4(S_{\omega}) \tag{28}$$

By equating relations Eqs (27) and (28), we get:

$$i_{sq-ref} = J\left(\dot{\omega}_{\text{ref}} + \frac{f}{J}\omega + K_4 \text{sig}(S_{\omega}) + 4(S_{\omega})\right) / \left(p\Phi_{rd}G\right) \tag{29}$$

Outer flux and speed loops SMC specifies the sliding surfaces for motor speed and rotor flux and retrieves the required reference current instructions (D-axis and Q-axis current references).

Figure 6 illustrates the diagram of the TFOC using SM controllers.

3.5. EFOC control using SM controller

3.5.1. Φ_{rq} Regulation

To improve the traditional sliding-mode controller-based control system, a third control loop can also be added, as in the improved control system based on PI controllers, to regulate the magnetic flux on the q-axis, thus avoiding magnetic saturation and improving motor operation. The switching function for the Φ_{rq} regulation loop can be written as follows:

$$S_q = \Phi_{\text{rq-ref}} - \Phi_{\text{rq}} \tag{30}$$

By deriving the previous relationship, and based on Eq. (13), we find:

$$\dot{S}_{\text{q}} = \dot{\Phi}_{\text{rq-ref}} + \left(\omega_s - \omega\right)\Phi_{\text{rd}} + a_1\Phi_{\text{rq}} \tag{31}$$

An adequate law of attraction must compensate for $\dot{S}_{\text{q}}$ to force the stream to travel towards the sliding surface:

$$\dot{S}_{\text{q}} = -K_5 \text{sig}(S_{\text{q}}) - Q_5(S_{\text{q}}) \tag{32}$$

By equating relations Eqs (31) and (32), we get:

$$\omega_s = \left(-a_1\Phi_{\text{rq}} - K_5 \text{sig}(S_{\text{q}}\right) - Q_5(S_{\text{q}})) / \Phi_{\text{rd}} + \omega \tag{33}$$

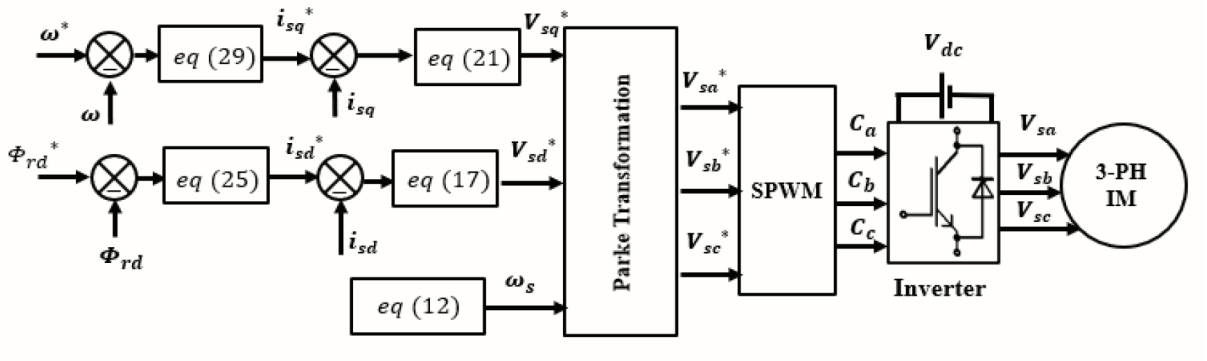

Figure 6. The illustration of TFOC using SM controllers. SPWM, sinusoidal pulse-width modulation; TFOC, traditional field-oriented control.

SMC for Q-axis flux regulation (EFOC-SM Strategy) defines the sliding surface and extracts the synchronous speed required to directly force the Q-axis flux to zero.

Figure 7 illustrates the diagram of EFOC using SM controllers.

The control parameters (K1, Q1, K2, Q2, K3, Q3, K4, Q4, K5 and Q5) were experimentally selected to achieve the best possible performance and improve the time response characteristics, namely minimising target overshoot and static error, taking into account that these constants must be positive and satisfy the condition (j).

4. Simulation Results

The motor speed was set at its nominal value of 152.8 rad · s^{-1}. Additionally, the reference value of the magnetic flux was set to its nominal value of 1.25 Wb. The nominal torque of 98 N · m^{-1} was applied at instant t = 2 s.

Under normal conditions, the temperature is assumed to be 25°C. However, during motor operation—especially under load—the temperature increases, and the winding temperature can reach values between 100°C and 125°C. This leads to an increase in the rotor winding resistance by approximately 35%–40%. Therefore, in this study, a resistance increase of 38% was assumed.

The physical basis for a 38% rotor resistance increase is based on the heat impact brought on by I^2R losses during loaded operation; a 38% increase in rotor resistance is assumed. The increase is connected to the anticipated temperature rise from the ordinary 25°C to the high working range of 100–125°C, which usually results in a resistance increase in the windings of around 35%–40%.

4.1. Simulation results of speed and torque response

Figure 8 illustrates the response of the studied control systems to speed regulation. It is observed that all control systems achieve effective performance in terms of tracking accuracy of the reference speed. However, it is worth noting that the two control systems based on sliding controllers achieve higher efficiency compared with the two control systems based on PICs under transient conditions. It is observed that the settling time using the EFOC-SM and TFOC-SM control systems is <0.1 s, followed by the EFOC-PI control system, which reaches 0.3 s, and finally the settling time using the TFOC-PI control system, which equals 0.4 s. It is also observed that the overshoot is zero when using the control systems using SMC, while the overshoot using the EFOC-PI control system is 4% and using TFOC-PI it is 6%. When the load torque is applied, it is observed that the speed decreases to 152.5 rad · s^{-1} using the SMC-based control systems and 147 rad · s^{-1} using the PIC-based control systems.

Sliding mode controller-based control systems also outperform in terms of reducing torque ripples, as shown in Figure 9. This is due to the effectiveness of the SMC methodology in terms of fast response and the ability to quickly process error signals in the current regulation loop, which contributes to improving torque response. The results shown in this figure indicate that the value of the torque peak-to-peak using the PIC-based control systems is equal to 13 N · m^{-1}, while it is equal to 3 N · m^{-1} using the TFOC-SM control system and to 0.3 N · m^{-1} using the EFOC-SM control system.

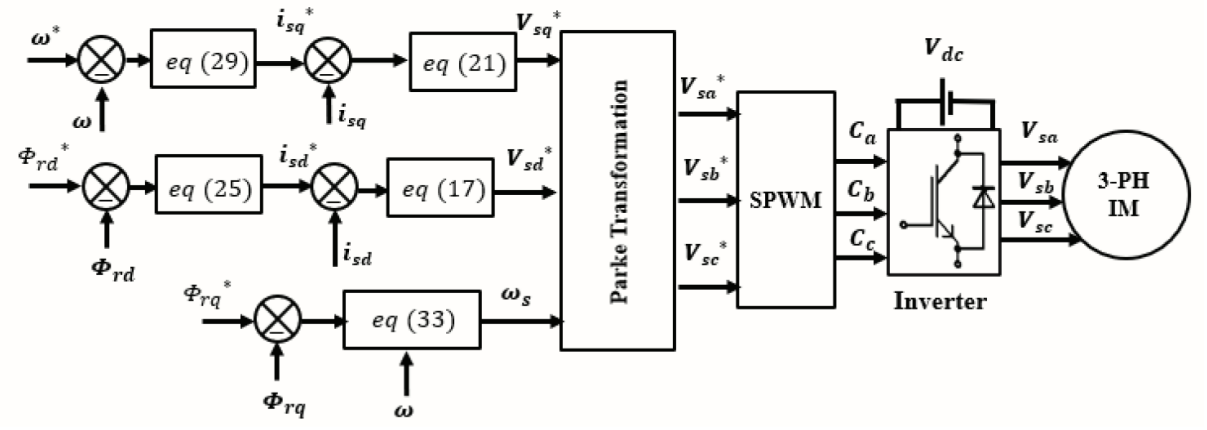

Figure 7. The illustration of EFOC using SM controllers. EFOC, enhanced field-oriented control; SPWM, sinusoidal pulse-width modulation.

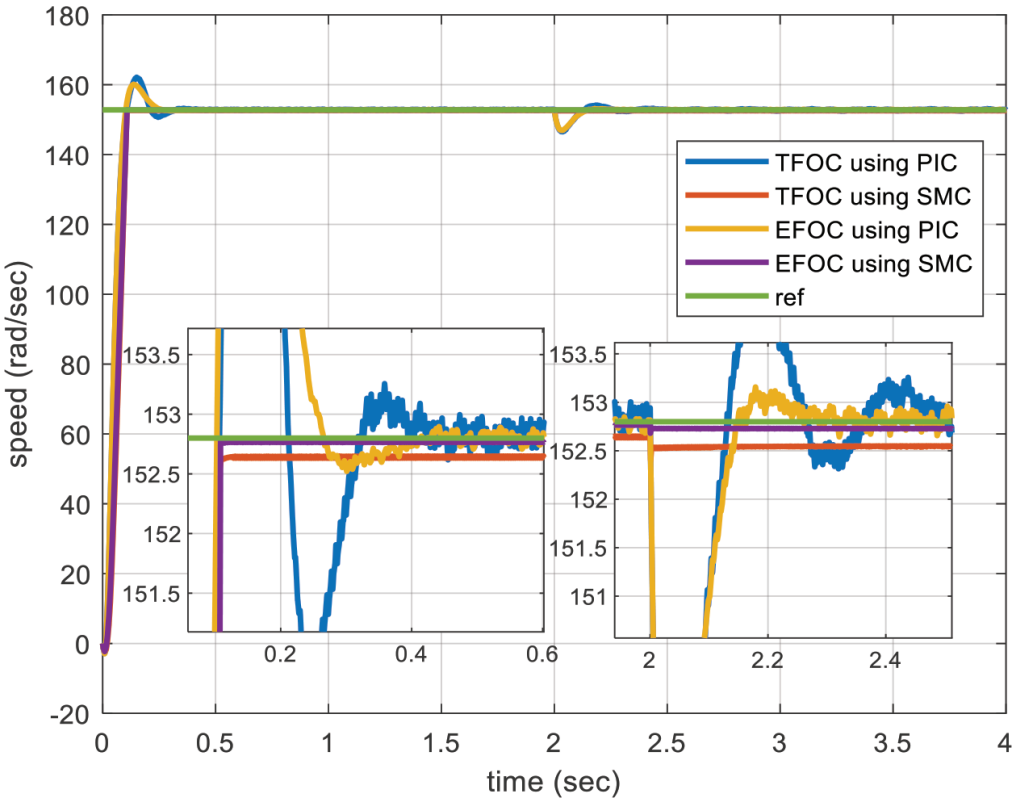

Figure 8. The response of the studied control systems for speed regulation. EFOC, enhanced field-oriented control; PIC, proportional-integral controller; SMC, sliding mode control; TFOC, traditional field-oriented control.

Standard performance indices, such as rise time, settling time and overshoot, were used to assess the system dynamics. According to the simulation results, the settling times for the TFOC–PI, EFOC–PI, TFOC–SM and EFOC–SM systems are roughly 0.4 s, 0.3 s, <0.1 s and <0.1 s, respectively, and the overshoot values are 6%, 4%, 0% and 0%. These findings validate that the sliding mode–based control systems (TFOC–SM and EFOC–SM) offer the fastest transient response with minimal overshoot, and outperform PI-based systems.

4.2. Simulation results of flux response

Regarding the regulation of the magnetic flux along both the d and q axes, the flux along the d-axis must maintain the nominal flux value, while the flux along the q-axis must be zero. Figures 9 and 10 show the response of the control systems to flux regulation along the d and q axes, respectively.

The results shown in Figure 10 indicate that all control systems achieve good and effective performance in tracking the reference value, with the two controlling systems based on the sliding mode controllers outperforming in transient cases, as they have a shorter settling time, lower overshoot and more robust against the load torque change. It is observed that the settling time using the EFOC-SM control system is <0.1 s, followed by the TFOC-SM control system, which reaches 0.15 s, and finally the settling time using the PIC-based control systems, which equals 0.5 s. It is also observed that the overshoot is zero when using the control systems using SMC, while the overshoot using the EFOC-PI control system is 0.05% and using TFOC-PI it is 1%. When the load torque is applied, it is observed that the flux increases to 1.29 wb using the TFOC-PI control system and 1.27 wb using the EFOC-PI control system, while it stays equal to 1.25 wb using the EFOC-SM control system and decreases to 1.24 wb using the TFOC-SM control system.

The results shown in Figure 11 clearly demonstrate the effectiveness of the EFOC-SM control system proposed in this research, which seeks to maintain the magnetic flux value on the q-axis near to zero, in the steady state, where a third regulation loop was added to achieve this, while it is noted that using traditional control systems, whether based on PIC or SMC, the flux value reaches the value of 0.42 wb before applying the load torque and 0.7 wb after that.

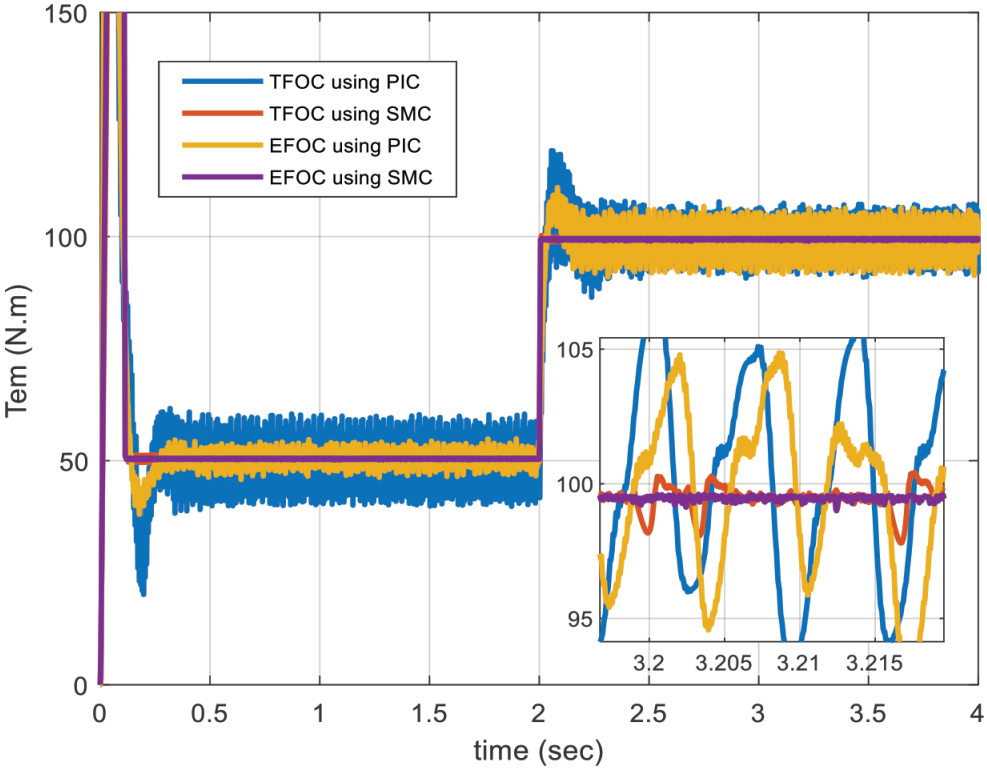

Figure 9. The torque response of the studied control systems. EFOC, enhanced field-oriented control; PIC, proportional-integral controller; SMC, sliding mode control; TFOC, traditional field-oriented control.

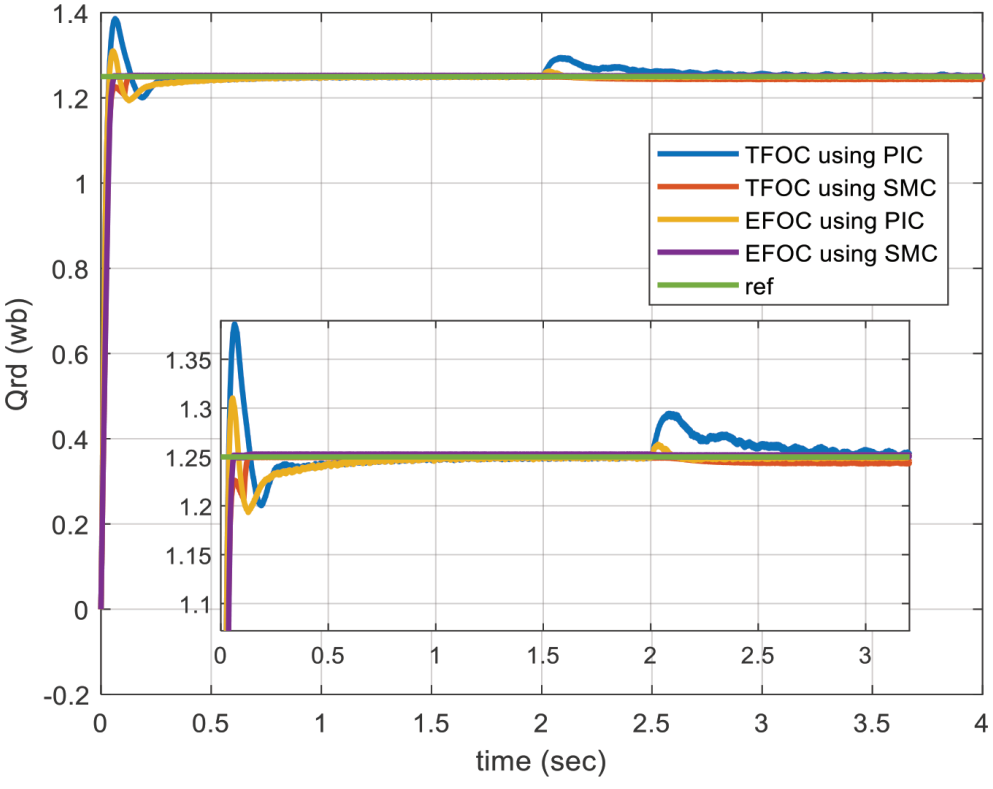

Figure 10. The flux on d-axis response of the studied control systems. EFOC, enhanced field-oriented control; PIC, proportional-integral controller; SMC, sliding mode control; TFOC, traditional field-oriented control.

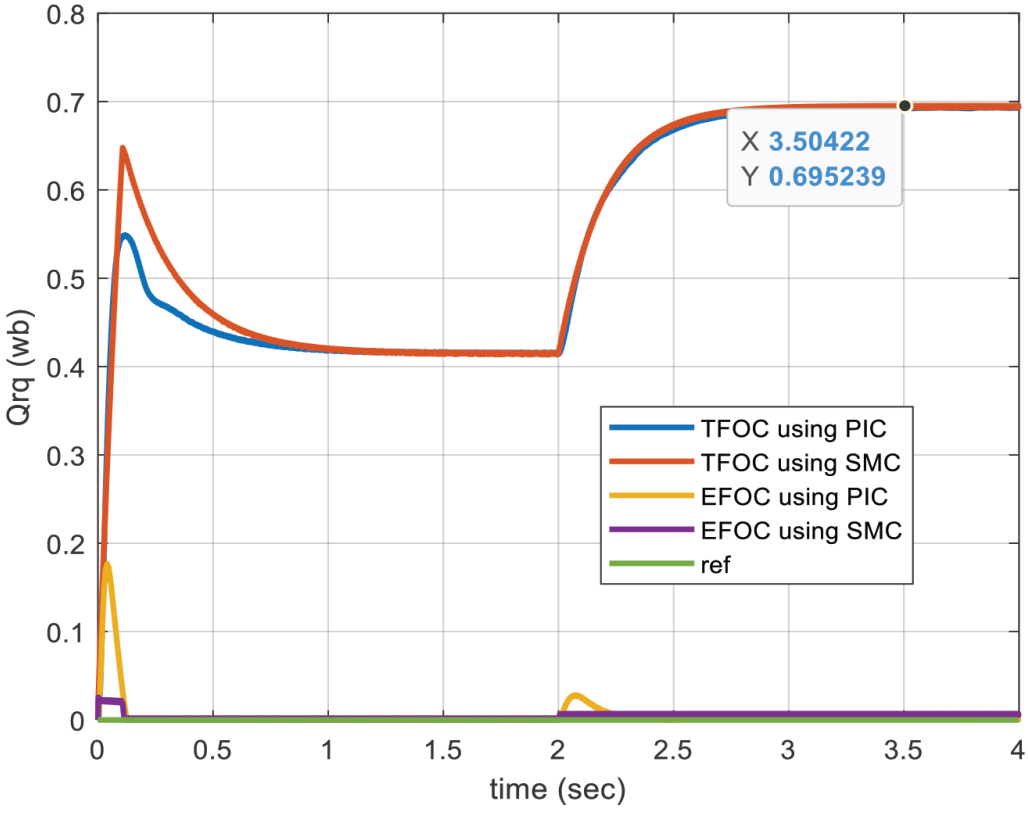

Figure 11. The flux on the q-axis response of the studied control systems. EFOC, enhanced field-oriented control; PIC, proportional-integral controller; SMC, sliding mode control; TFOC, traditional field-oriented control.

4.3. Simulation results of voltage and frequency

Figures 12 and 13 show the voltage and electrical frequency applied to the motor for the studied control systems.

It is noted from Figures 12 and 13 that the two traditional control systems (either based on PIC or SMC) produce a higher voltage and a lower frequency compared with the two enhanced control systems, which causes a higher magnetic flux value.

4.4. Simulation results of the power response

Increasing the magnetic flux value will cause an increase in the reactive power consumed by the motor, keeping in mind, of course, that the active power is not really affected by the increase in magnetic flux, as shown in Figures 14 and 15.

The active power consumed after applying the load torque is 16.2 kW, but it is very important to note that the reactive power is 10.9 kVAR when using conventional control systems, while it is 8.8 kVAR when using improved control systems, which means an improvement in the power factor, as shown in Figure 16. It is noted that the amount of improvement in the power factor value is approximately 5.5% for applying a torque load equal to zero, and approximately 7% for applying a torque load equal to the nominal value.

4.5. Analytical study of the FOC system

The effectiveness and benefit of the enhanced control system lie in maintaining the magnetic flux at zero by correctly generating the voltage and frequency values, unlike the traditional control system.

The main problem with the traditional control system is that the frequency is calculated using Eq. (12), assuming that the magnetic flux on the q-axis is zero. So, it can be said that the regulation of the magnetic flux on the q-axis is done indirectly.

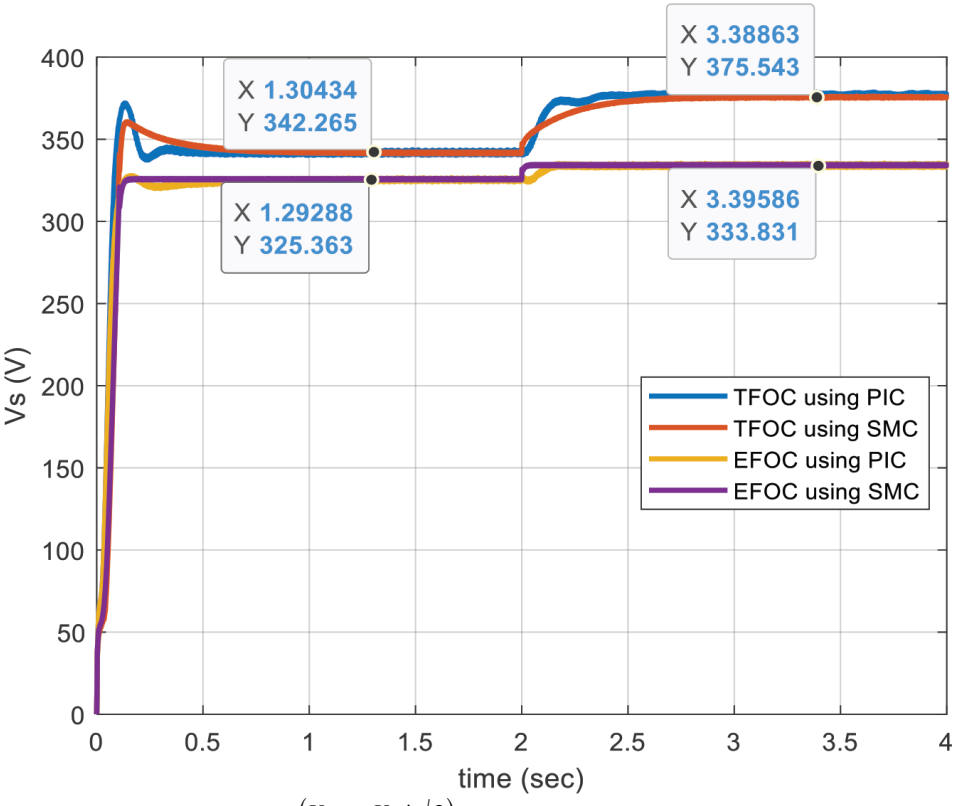

Figure 12. The voltage applied $\left(V_{max} = V_{ph} * \sqrt{2}\right)$ on the motor for the studied control systems. EFOC, enhanced field-oriented control; PIC, proportional-integral controller; SMC, sliding mode control; TFOC, traditional field-oriented control.

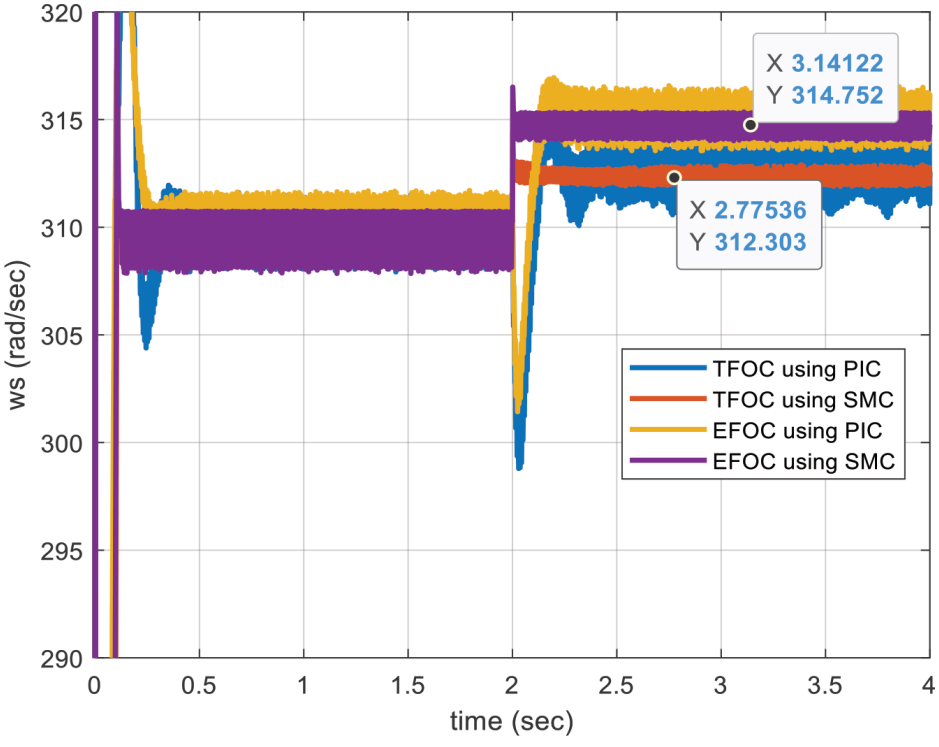

Figure 13. The electrical frequency applied to the motor for the studied control systems. EFOC, enhanced field-oriented control; PIC, proportional-integral controller; SMC, sliding mode control; TFOC, traditional field-oriented control.

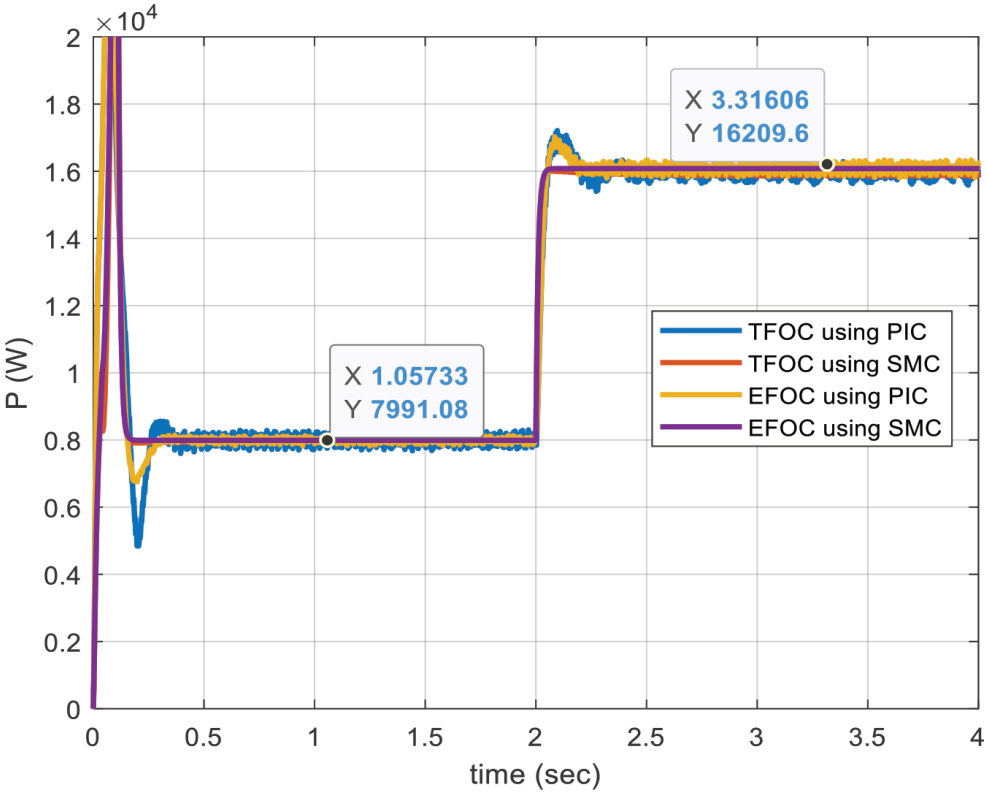

Figure 14. The active power consumed using the studied control systems. EFOC, enhanced field-oriented control; PIC, proportional-integral controller; SMC, sliding mode control; TFOC, traditional field-oriented control.

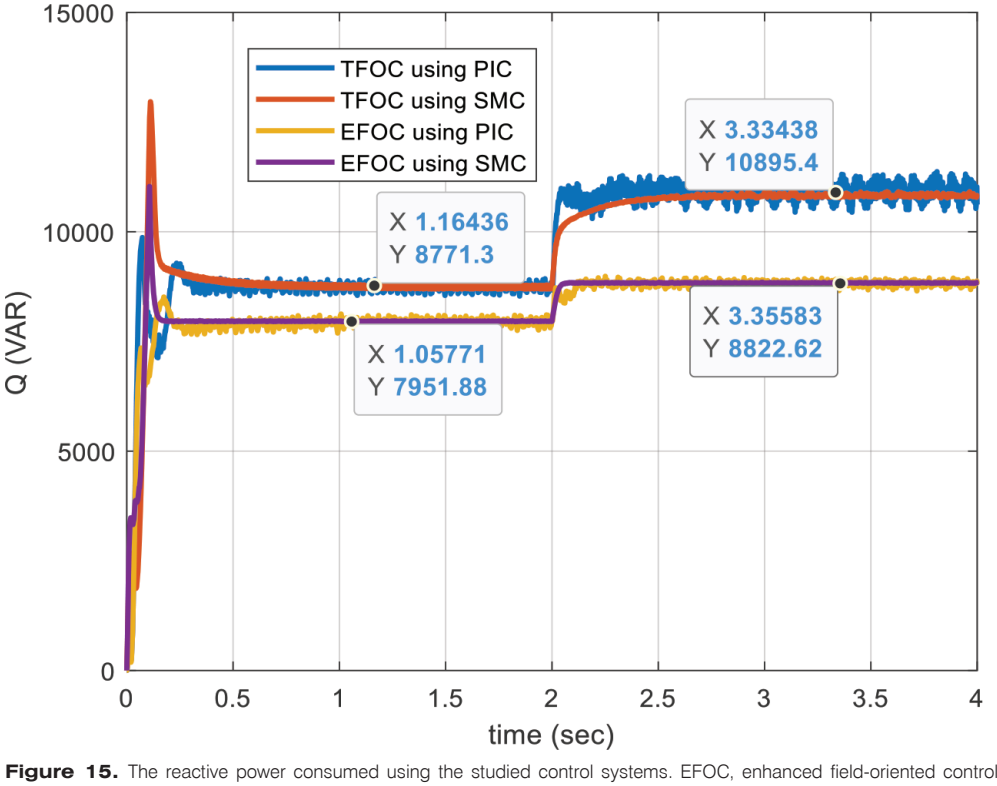

Figure 15. The reactive power consumed using the studied control systems. EFOC, enhanced field-oriented control; PIC, proportional-integral controller; SMC, sliding mode control; TFOC, traditional field-oriented control.

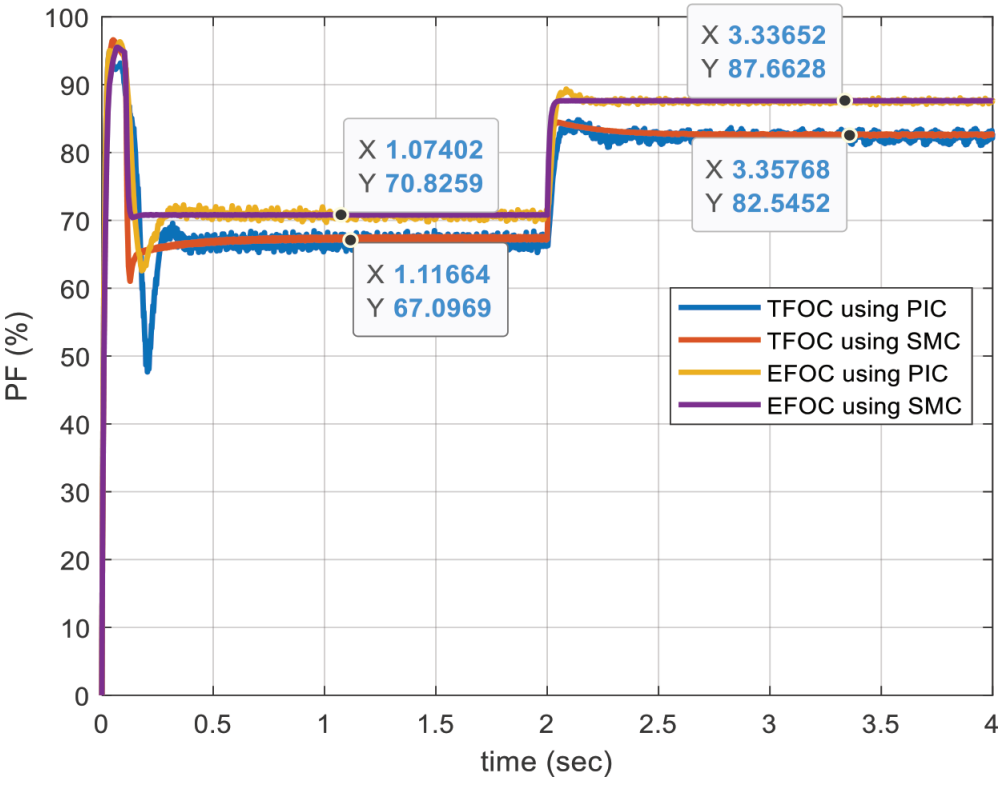

Figure 16. The reactive power consumed using the studied control systems. EFOC, enhanced field-oriented control; PIC, proportional-integral controller; SMC, sliding mode control; TFOC, traditional field-oriented control.

This equation shows that by increasing the rotor resistance value, the frequency must be increased. Therefore, if the rotor resistance value is increased without taking this into account within Eq. (12), the frequency will be lower than it should be, which causes the flux value on the q-axis to increase. However, in the enhanced control system, where a third loop is added to regulate the flux—the regulation of the magnetic flux on the q-axis is done directly—this problem is overcome by generating the appropriate frequency to achieve this goal.

Table 3 shows a numerical comparison between the performance of the conventional control system and the improved control system. The improved control system reduces the voltage and frequency, maintaining the magnetic flux at its nominal value. This contributes to improving the power factor and reducing the reactive power consumed. Table 5 shows a comparison between the four systems in terms of the performance criteria studied during the research. By reviewing the results in Figures 7–15, it is observed that the improved control system based on the sliding mode outperforms in reducing torque ripples, is more effective in overcoming load torque variations, and reduces settling time.

The decoupling of flux components, which reduces cross-coupling effects between the d- and q-axes, and the design of the sliding surface, which guarantees quicker error convergence, are responsible for the improved transient performance of the augmented control system.

The trade-offs have also been discussed: the suggested system offers a notable gain in torque responsiveness and dynamic stability, but it also introduces a small amount of computational complexity due to the additional control loops. Additionally, by using a boundary layer approach, the chattering phenomena related to SMC have been successfully reduced.

4.6. Economic effect analysis

In addition to enhancing the induction motor's dynamic and steady-state performance, the suggested EFOC system has major financial advantages. The system reduces energy losses by lowering reactive power consumption and improving flux regulation efficiency, which immediately lowers operational costs. Additionally,

Table 3. Parameters of the studied motor.

R_s	0.2147 Ω
R_r	0.2205 Ω
L_s	0.065181 H
L_r	0.065181 H
L_m	0.06419 H
J	0.1 kg · m^{-2}
F	0.0095 kg · m^{-2} · s^{-1}
P	2
Nominal power	15 kW
Nominal phase voltage	230 V
Nominal synchronous speed	314 rad · s^{-1}
Nominal mechanical speed	152.8 rad · s^{-1}

Table 4. Combined performance overview of examined control systems.

Control system	Settling time (s)	Overshoot (%)	Torque tipple (N • m^{-1})	Power factor improvement (%)	Remarks/ observation
TFOC–PI	0.4	6	13	–	Conventional PI-based FOC shows slower response and higher ripple.
EFOC–PI	0.3	4	13	~ 6	Added q-axis flux regulation improves stability and PF slightly.
TFOC–SM	<0.1	0	3	~ 6	Sliding mode enhances transient response and reduces ripple.
EFOC–SM	<0.1	0	0.3	7	Proposed system achieves fastest response, lowest ripple, and best PF.

EFOC, enhanced field-oriented control; FOC, field-oriented control; PI, proportional-integral; TFOC, traditional field-oriented control.

Table 5. Power and electrical parameters at rated load.

Criterion	Traditional control system	Enhanced control system	Enhancement (%)
Voltage (V)	375	333.4	Reduce 11
Frequency (Hz)	312.3	315	Increase 0.85
Regulations Φ_rq	Indirect	Direct	-
Rotor flux (wb)	1.43	1.25	Reduce 12
Active power (kW)	16.2	16.2	-
Reactive power (kVAR)	10.9	8.8	Reduce 20
Power factor	0.83	0.88	Increase 6

Table 6. Control performance comparison.

Performance metric		EFOC-PI	TFOC-PI	EFOC-SM	TFOC-SM
Speed regulation	Settling time (s)	0.3	0.4	<0.1	<0.1
	Overshoot (%)	4	6	0	0
	Speed value at the moment of applying torque (rad · s^{-1})	147	147	152.5	152.5
Torque ripple	(Peak-to-peak) (N · m^{-1})	13	13	0.3	3
Flux—d axis	Settling time (s)	0.5	0.5	<0.1	0.15
	Overshoot (flux—d axis) (%)	0.05	1	0	0
	Flux value at the moment of applying the torque (Wb)	1.27	1.29	1.25	1.24
Flux—q axis	(Steady state) (Wb)	≈0	0.42 → 0.7	≈0	0.42 → 0.7

EFOC, enhanced field-oriented control; PI, proportional-integral; SM, TFOC, traditional field-oriented control.

smoother operation and less thermal stress on components result from the enhanced stability and resilience against rotor resistance changes.

With a conventional drive system, as previously observed from the results, any change in rotor resistance value will cause the magnetic flux to exceed its nominal value. This increase in flux is what causes the machine to heat up more compared with the case of using an advanced drive system that keeps the flux within the nominal limits despite the change in rotor resistance value.

Reduced maintenance frequency and system downtime are the outcomes of this longer component lifespan. As a result, as compared with traditional FOC schemes, the EFOC-based design offers an economical and energy-efficient approach that enhances both technical performance and long-term system sustainability.

4.7. Computational complexity and comparative analysis

A quick examination of the computational complexity and system sensitivity has been included to the updated version. Since the suggested EFOC structure mainly uses PI and sliding mode controllers without necessitating lengthy optimisation or learning procedures, it retains a minimal computing cost. The suggested approach provides a good compromise between control precision, real-time practicality and implementation simplicity when compared with sophisticated control techniques like model predictive control (MPC) and artificial intelligence (AI)-based methods like reinforcement learning (RL). In order to further improve system performance and lessen susceptibility to parameter fluctuations, future work will concentrate on combining adaptive and AI-based algorithms.

5. Conclusion

This research developed an enhanced FOC system to enhance the steady-state performance of an induction motor and overcome the problem of rotor resistance variations. This was achieved by adding a third control loop to the traditional FOC system, through which the magnetic flux on the q-axis is regulated to ensure that its value remains at zero. In the second stage, the control system was developed using a sliding mode technique, which enhanced the system's transient performance. This also contributed to reducing torque ripples and increasing the system's robustness to external disturbances.

The results of this research demonstrate that the SMC-based enhanced control system clearly outperforms traditional control systems, whether they rely on PIC or SMC. The enhanced system is characterised by its faster response and better magnetic regulation, particularly in maintaining the q-axis magnetic flux at zero in the steady state, although there is a change in the rotor resistance value.

The most notable indicators confirming the effectiveness of the SMC-based enhanced control system include as follows:

- High transient performance: Shorter settling time, reduced overshoot and greater robustness to load torque changes.
- Reduced torque ripple: the peak-to-peak torque using SMC-based control systems is 0.3–3 $N \cdot m^{-1}$, while it equals 13 $N \cdot m^{-1}$ using PIC-based control systems, taking into account that the nominal torque is equal to 98 $N \cdot m^{-1}$.
- Generating correct voltage and frequency values despite rotor resistance changes.
- Reduced reactive power consumption, thus improving the power factor by up to 7% at nominal load.

There are still certain restrictions even though the suggested EFOC system based on SMC exhibits better transient performance, better flux regulation and fewer torque ripples. The work is restricted to simulation-based validation, which could not accurately represent measurement noise, parameter fluctuations and inverter non-linearities in actual systems. Furthermore, high-frequency switching in SMC may cause a small amount of chattering. In order to increase smoothness, robustness and energy efficiency, future research should include advanced chattering reduction or hybrid adaptive–sliding mode controllers; adaptive or observer-based parameter estimation to handle resistance fluctuations; and real-time experimental verification.

References

Abed, K. and Zine, H. K. E. (2024). Intelligent Fuzzy Back-Stepping Observer Design Based Induction Motor Robust Nonlinear Sensorless Control. *Electrical Engineering and Electromechanics*, 2024(2), pp. 10–15. doi: 10.20998/2074-272X.2024.2.02

Alaa, T. and Temurtaş, F. (2024). Enhanced Fuzzy Logic Control Model and Sliding Mode Based on Field Oriented Control of Induction Motor. *World Journal of Engineering and Technology*, 12(1), pp. 65–79. doi: 10.4236/wjet.2024.121004

Ali, S., Prado, A. and Pervaiz, M. (2023). Hybrid Backstepping-Super Twisting Algorithm for Robust Speed Control of a Three-Phase Induction Motor. *Electronics (Switzerland)*, 12(3), pp. 1–27.

Azzoug, Y., Sahraoui, M., Pusca, R., Ameid, T., Romary, R. and Cardoso, A. J. M. (2021). High-Performance Vector Control without AC Phase Current Sensors for Induction Motor Drives: Simulation and Real-Time Implementation. *ISA Transactions*, 109, pp. 295–306. doi: 10.1016/j.isatra.2020.09.021

Benderradji, H., Benaicha, S. and Alaoui, L. C. (2025). Improved Sliding Mode Control for Induction Motor Based on Twisting Algorithm. *AIMS Electronics and Electrical Engineering*, 9(1), pp. 81–98. doi: 10.3934/electreng.2025005

Do, T. D., Le, N. D., Phuong, V. H. and Lam, N. T. (2022). Implementation of FOC Algorithm Using FPGA for GaN-Based Three-Phase Induction Motor Drive. *Bulletin of Electrical Engineering and Informatics*, 11(2), pp. 636–645. doi: 10.11591/eei.v11i2.3569

El Bourhichi, S., Oukassi, A., El Bahir, L. and El Adnani, M. (2021). Active Disturbance Rejection Control for a Five-Level Cascaded H-Bridge Inverter Fed Induction Motor Sensorless Field-Oriented. *Mathematical Problems in Engineering*, 2021. doi: 10.1155/2021/9925072

Faizal, A. A., et al. (2023). Direct Torque Control (DTC) Design With Fuzzy Sugeno-Proportional Derivative for 3-Phase Induction Motor Speed Control. *Journal Ecotipe (Electronic, Control, Telecommunication, Information, and Power Engineering)*, 10(1), pp. 111–120. doi: 10.33019/jurnalecotipe.v10i1.3925

Fereka, D., Zerikat, M. and Belaidi, A. (2018). MRAS sensorless speed control of an induction motor drive based on fuzzy sliding mode control. In: *2018 7th International Conference on Systems and Control, ICSC*. pp. 230–236.

Horch, M., Boumédiène, A. and Baghli, L. (2019). Direct Torque Control of Induction Machine Drive Based on Sliding Mode Controller and a Stator Resistance Compensator With a New Hybrid Observer. *International Journal of Digital Signals and Smart Systems*, 3(1–3), pp. 60–78. doi: 10.1504/IJDSSS.2019.103384

Kumar, G. and Mehar, V. (2022). Efficient Field-Orientation Control Technique for Induction Motor-Based Applications. *Research Journal of Engineering Technology and Medical Sciences*, 05(4), pp. 40–48.

Liu, P. and Hao, L. (2006). Vector Control-Based Speed Sensorless Control of Induction Motors Using Sliding-Mode Controller. *Proceedings of the World Congress on Intelligent Control and Automation (WCICA)*, 1(3), pp. 1942–1946. doi: 10.1109/WCICA.2006.1712695

Mahmood, A. S. (2024). Enhancing Performance of Photovoltaic Pump Systems in Remote Areas Using a Sliding Mode Technique for Maximum Power Point Tracking. *Progress In Electromagnetics Research B*, 104, pp. 131–146. doi: 10.2528/PIERB23110206

Mahmood, A. S. and Teke, M. (2023). Improving the Efficiency of Solar Systems by Tracking the MPP under Different Test Conditions. *Progress In Electromagnetics Research B*, 99, pp. 83–102. doi: 10.2528/PIERB23010703

Mahmood, A. S., Teke, M., Ibrahim, R. K., Ali, A. H., Abdulrazzaq, A. A. and Kareem, M. M. (2022). Tracking the MPP of a PV system using an advanced fuzzy logic control technique. In: *2022 2nd International Conference on Advances in Electrical, Computing, Communication and Sustainable Technologies, ICAECT*.

Marčetić, D. P. and Vukosavić, S. N. (2007). Speed-Sensorless AC Drives With the Rotor Time Constant Parameter Update. *IEEE Transactions on Industrial Electronics*, 54(5), pp. 2618–2625. doi: 10.1109/TIE.2007.899880

Mennad, M., Abderrahim, B. and Youcef, D. (2024). Enhancing Performance and Optimizing Energy Utilization and Voltage Regulation in Hybrid Wind-Solar Pumping Systems. *Journal Europeen des Systemes Automatises*, 57(4), pp. 1035–1045. doi: 10.18280/jesa.570411

Online and Citation. (2024). Optimizing Energy Transmission Quality from Photovoltaic. p. 050014.

Peng, K. and Zhao, J. (2011). Speed control of induction motor using neural network sliding mode controller. In: *2011 International Conference on Electric Information and Control Engineering, ICEICE – Proceedings*. pp. 6125–6129.

Rahmatullah, R., Ayca, A. K. and Serteller, N. F. O. (2023). Design of Sliding Mode Control Using

SVPWM Modulation Method for Speed Control of Induction Motor. *Transportation Research Procedia*, 70, pp. 226–233. doi: 10.1016/j.trpro.2023.11.023

Ramzi, T., Adel, K., Mimouni, M. F. and M'Sahli, F. (2012). Backstepping Control for an Induction Motor Using an Adaptive Sliding Rotor-Flux Observer. *Electric Power Systems Research*, 93, pp. 1–15. doi: 10.1016/j.epsr.2012.06.004

Shaija, P. J. and Daniel, A. E. (2021). Robust sliding mode control strategy applied to IFOC induction motor drive. In: *2021 4th International Conference on Electrical, Computer and Communication Technologies, ICECCT*. pp. 1–6.

Shiravani, F., Patxi, A., Cortajarena, J. A. and Barambones, O. (2023). An Improved Predictive Current Control for IM Drives. *Ain Shams Engineering Journal*, 14(8), p. 102037. doi: 10.1016/j.asej.2022.102037

Sudaryanto, A., Purwanto, E., Ferdiansyah, I., Nugraha, S. D., Qudsi, O. A. and Rifadil, M. M. (2020). Design and implementation of SVPWM inverter to reduce total harmonic distortion (THD) on three-phase induction motor speed regulation using constant V/F. In: *2020 3rd International Seminar on Research of Information Technology and Intelligent Systems, ISRITI*. pp. 412–417.

Sultan, A. H. and Al-Badrani, H. (2024). Field oriented control for seven phase induction machine with comparative control method. In: *12th International Conference on Smart Grid, icSmartGrid 2024*. pp. 844–849.

Swargiary, M., Dey, J. and Saha, T. K. (2016). Optimal speed control of induction motor based on linear quadratic regulator theory. In: *12th IEEE International Conference on Electronics, Energy, Environment, Communication, Computer, Control: (E3-C3), INDICON 2015*. pp. 1–6.